Scalar Quantization Error Analysis for Image Subband Coding Using QMF's

Peter H. Westerink, *Member, IEEE*, Jan Biemond, *Senior Member, IEEE*, and Dick E. Boekee, *Associate Member, IEEE*

Abstract—**Filter design for signal splitting and reconstruction in subband coding is based in practice on the assumption that coding errors are negligible. In the absence of coding the aliasing errors are explicitly canceled when quadrature mirror filters (QMF's) are used. The fact that aliasing errors occur in the presence of coding errors is acknowledged in the literature. However, no quantitative evaluation has been made so far. This paper explicitly incorporates quantization errors into a QMF system by means of a quantizer model. This enables us to discriminate between different types of coding errors, such as the aliasing error. Other distinguished errors are a QMF design error, a signal error, and a random error, which is uncorrelated with the original image. Both a mean-squared error calculation and a subjective judgement of the coding errors show that the aliasing errors can be neglected for filter lengths of 12 taps or more. The signal error determines the sharpness of the reconstructed image, while the random error is most visible in the flat areas.**

I. Introduction

THE basic idea of subband coding is to split up the frequency band of the signal and to code each subband separately using a coder and bit rate closely matched to the statistics of that particular band. However, splitting the signal into subbands basically involves digital FIR or IIR bandpass filtering followed by downsampling. As a result, aliasing will occur in the subbands and special care has to be taken to reconstruct the signal in order not to let the reconstruction suffer from aliasing error effects. By applying special techniques, such as the quadrature mirror filter (QMF) technique [4], the conjugate quadrature filter (CQF) technique [8], or an IIR filtering technique [1], the aliasing errors are explicitly canceled out in the reconstruction stage. These methods, however, have been developed under the assumption that coding errors are negligible, while in practice, in subband coding, we always have coding errors due to the encoding and decoding of the subbands. In that case the aliasing errors will not completely be canceled out in the reconstruction. The occurrence of these aliasing errors due to coding is acknowledged in the literature. For instance, in [7] a remark is made on the occurrence of aliasing errors due to speech coding, the severity depending on the coding accuracy. In [2] a thorough comparison between different filters and filter techniques for image coding is made with respect to their coder performance. However, sofar neither has an actual analysis yet been made of the aliasing errors, nor has been investigated whether the assumption of neglecting the coding errors for filter design is justified for images.

It is the purpose of this paper to analyze the coding errors due to quantization by explicitly incorporating a mathematical model for a Lloyd–Max quantizer into a QMF splitting and reconstruction scheme [12]. Although other filter techniques to split a signal into subbands exist, in this paper we will confine ourselves to the QMF technique. Also, we will apply Lloyd–Max quantizers to encode the spatial domain subbands, this in contrast to [2], where uniform threshold quantizers are being used. To describe the Lloyd–Max quantizer we will use a model that is known as the "gain-plus-additive-noise quantizer model" [6] which will turn out to be very convenient for our purpose. Not only does this model fit very well to the actual data but, moreover, we are also able to classify the coding errors due to quantization into different types of errors, among which is the aliasing error, and gain more insight into the specific nature of subband coding errors. In this manner we can investigate the impact of the aliasing errors (among others) on the final subband coding result, and consider their severity.

II. The Gain-Plus-Additive-Noise Quantizer Model

The basic intention of introducing a quantizer model into a QMF splitting and reconstruction scheme is to derive an input/output relation for the total system, in which the coding errors are incorporated. We would like to use a (simple) model where the quantizer output is made up of parts that are independent or uncorrelated with each other. Using such a model, we then expect to be able to split up the total reconstruction error into different classes of errors.

The obvious model for this purpose would be the fairly common additive input-independent noise quantizer model

$$y = x + q \tag{1}$$

Manuscript received October 30, 1989; revised December 18, 1990.

P. H. Westerink was with the Department of Electrical Engineering, Information Theory Group, Delft University of Technology, 2600 GA Delft, the Netherlands. He is now with Panasonic Technologies, Inc., Burlington, NJ 08016.

J. Biemond and D. E. Boekee are with the Information Theory Group, Department of Electrical Engineering, Delft University of Technology, 2600 GA Delft, the Netherlands.

IEEE Log Number 9104884.

where the input signal x and the additive noise q are uncorrelated [6]. The model is also shown in Fig. 1(a). Note that this is the model that is being used in [2] to describe a uniform threshold quantizer, where the quantization noise q is assumed to be independent of the signal x and uniformly distributed. By squaring and taking the expectations of (1) we get

$$E[y^2] = E[(x + q)^2] = E[x^2] + 2E[xq] + E[q^2] \quad (2)$$

and because the noise q is assumed to be uncorrelated with the input signal x, that is, $E[xq] = 0$, we get

$$\sigma_y^2 = \sigma_x^2 + \sigma_q^2. \quad (3)$$

In this simple model therefore, the variance of the quantizer output is larger than that of the input.

However, in [6] it is shown that for the Lloyd–Max quantizers we are using to encode the subbands it holds that

$$\sigma_y^2 = \sigma_x^2 - \sigma_q^2 \quad (4)$$

and the assumption of additive uncorrelated noise turns out to be incorrect. In order to satisfy (4) and have uncorrelated additive noise, a better model for Lloyd–Max quantization is therefore not a purely additive uncorrelated noise model, but one with a less-than-unity gain component and an additive component, according to

$$y = \alpha x + r. \quad (5)$$

This model is shown in Fig. 1(b), where α is the multiplication (gain) factor such that αx represents the signal part of the quantized signal y and r is the uncorrelated additive noise term. Using this model, we can now show that by making a proper choice for the gain α the assumption of an additive uncorrelated noise signal r can be justified.

For Lloyd–Max quantizers it can be shown that the quantization noise q is orthogonal to the output y of the quantizer [6], or, equivalently, $E[qy] = 0$. Using this orthogonality property we then first calculate

$$E[xq] = E[(y - q)q] = E[yq] - E[q^2] = -\sigma_q^2 \quad (6)$$

and next

$$E[xq] = E[x(y - x)] = E[x(\alpha x + r - x)] = (\alpha - 1)\sigma_x^2 + E[xr]. \quad (7)$$

Finally, by deliberately setting the correlation between the input signal x and the additive noise r equal to zero, that is, $E[xr] = 0$, and equating (6) and (7), we obtain

$$\alpha = 1 - \frac{\sigma_q^2}{\sigma_x^2}. \quad (8)$$

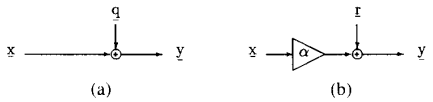

Fig. 1. Quantizer models: (a) additive input-independent noise model, and (b) model with nonunity gain and additive noise.

Note that the value $\sigma_q^2 = E[(y - x)^2]$ is the mean-squared error of the Lloyd–Max quantizer. Therefore, α is equal to one minus the normalized quantizer distortion; in general this value is known after quantizer design. Thus, if we choose α according to (8), the additive noise will be uncorrelated to the input signal. In fact, this is the main attractive feature of this model and the reason we want to incorporate this model into the QMF system.

The variance of the uncorrelated noise signal is finally calculated by

$$E[y^2] = E[(\alpha x + r)^2] = \alpha^2\sigma_x^2 + \sigma_r^2 \quad (9)$$

and by using (4) and (8) we finally obtain

$$\sigma_r^2 = (1 - \alpha^2)\sigma_x^2 - \sigma_q^2 = \alpha(1 - \alpha)\sigma_x^2. \quad (10)$$

As was to be expected, the random noise variance σ_r^2 will be zero in two cases: 1) there are no coding errors, $\sigma_q^2 = 0.0 \Rightarrow \alpha = 1.0$, and 2) the signal is "encoded" with just its mean value, σ_q^2 and $\sigma_x^2 \Rightarrow \alpha = 0.0$.

III. Incorporation of the Quantizer Model into a 1D QMF Scheme

In the elementary 1D QMF filter scheme the 1D signal is split into two subbands by first bandpass filtering the signal and then decimating the result by a factor 2. In the frequency domain this operation can be described by

$$X_i(\omega) = \frac{1}{2}\sum_{k=0}^{1} H_i\left(\frac{\omega}{2} + k\pi\right) X\left(\frac{\omega}{2} + k\pi\right) \quad (11)$$

where $X(\omega)$ is the input signal and $X_i(\omega)$ for $i = 0, 1$, are the two separate subbands. Here the QMF filters $H_0(\omega)$ and $H_1(\omega)$ are each other's shifted equivalents, according to

$$H_0(\omega) = H(\omega) \quad (12)$$

$$H_1(\omega) = H(\omega + \pi). \quad (13)$$

The reconstruction of the 1D signal is performed, respectively, by upsampling with a factor 2, suitably bandpass filtering and adding the subbands. In the QMF approach the reconstruction can be written as

$$\hat{X}(\omega) = 2\sum_{i=0}^{1} (-1)^i H_i(\omega)\hat{X}_i(2\omega) \quad (14)$$

where $\hat{X}_i(\omega)$ are the subband signals after encoding/decoding. Although present filter design is based on neglecting the coding errors, that is, assuming that $\hat{X}_i(\omega) \equiv X_i(\omega)$

for $i = 0, 1$, in practice $\hat{X}_i(\omega)$ will not be equal to $X_i(\omega)$. Therefore, in order define an appropriate relation between coder input and coder output, from now on we will assume that we quantize the subbands $X_0(\omega)$ and $X_1(\omega)$ in the spatial domain (that is, we quantize $x_0(n)$ and $x_1(n)$) using a Lloyd–Max quantizer. In that case we can use the quantizer model as derived in the previous section and describe the two subband coders/decoders using the Fourier equivalent of the model of (5):

$$\hat{X}_i(\omega) = \alpha_i X_i(\omega) + R_i(\omega) \tag{15}$$

for $i = 0, 1$. Combining (11), (14), and (15) we can now write the input/output relation of the 1D QMF system with Lloyd–Max quantization as

$$\begin{aligned}\hat{X}(\omega) = {} & X(\omega) \sum_{i=0}^{1} (-1)^i \alpha_i H_i(\omega) H_i(\omega) \\ & + X(\omega + \pi) \sum_{i=0}^{1} (-1)^i \alpha_i H_i(\omega) H_i(\omega + \pi) \\ & + \sum_{i=0}^{1} (-1)^i H_i(\omega) R_i(2\omega).\end{aligned} \tag{16}$$

In this equation we can distinguish three different additive parts:

1) a signal part (the first summation), which is a filtered version of $X(\omega)$,
2) an aliasing part (the second summation), which is a filtered version of $X(\omega + \pi)$, and
3) a random part (the third summation), uncorrelated with the signal $X(\omega)$.

Starting from this observation we first define the reconstruction error $E(\omega)$ as the difference between the reconstructed signal $\hat{X}(\omega)$ and the original input signal $X(\omega)$:

$$E(\omega) = \hat{X}(\omega) - X(\omega). \tag{17}$$

Next, we subdivide the reconstruction error into four typical error signals:

$$E(\omega) = E_Q(\omega) + E_S(\omega) + E_A(\omega) + E_R(\omega) \tag{18}$$

where

$E_Q(\omega)$ QMF design error, which always occurs,
$E_S(\omega)$ signal error,
$E_A(\omega)$ aliasing error, and
$E_R(\omega)$ random error, uncorrelated with the signal $X(\omega)$.

The equations for each of the errors are easily derived from (16) and are given by

$$E_Q(\omega) = [H(\omega)^2 - H(\omega + \pi)^2 - 1] X(\omega) \tag{19}$$

$$E_S(\omega) = [(\alpha_0 - 1) H(\omega)^2 - (\alpha_1 - 1) H(\omega + \pi)^2] X(\omega) \tag{20}$$

$$E_A(\omega) = [(\alpha_0 - \alpha_1) H(\omega) H(\omega + \pi)] X(\omega + \pi) \tag{21}$$

$$E_R(\omega) = 2H(\omega) R_0(2\omega) - 2H(\omega + \pi) R_1(2\omega). \tag{22}$$

It can be clearly seen that we now have separated the aliasing error signal within the total reconstruction error, thus allowing a quantitative evaluation of the aliasing errors. Note, that except for $E_R(\omega)$ the three other error signals need not necessarily be uncorrelated, although experimental results as presented later in the paper indicate highly uncorrelated signals. By choosing this particular subdivision into different errors we can examine different coding error artifacts, among which is the aliasing error. By definition, in the absence of coding errors only $E_Q(\omega)$ remains, since in that case $\alpha_0 = \alpha_1 = 1$ and $\sigma_{R_0}^2 = \sigma_{R_1}^2 = 0$. In the presence of quantization errors, however, in general the errors $E_S(\omega)$, $E_A(\omega)$, and $E_R(\omega)$ are not zero and are dependent on the type of filter $H(\omega)$ used, the input signal $X(\omega)$ and the bit allocation, which determines the values of α_i and thus $\sigma_{R_i}^2$. Note that in the case where both subbands are encoded using the same quantizer, we will have identical values for α_0 and α_1 and the aliasing errors will be eliminated.

IV. The Extension to 2D

In this section we will make the extension of 1D to 2D. Again we assume that we have Lloyd–Max quantizers that can be modeled by the gain-plus-additive-noise model. Combining the 2D equations for splitting, quantization and reconstruction is straightforward, and results in the 2D input/output relation

$$\begin{aligned}\hat{X}(\omega_0, \omega_1) = {} & \sum_{k=0}^{1} \sum_{l=0}^{1} X(\omega_0 + k\pi, \omega_1 + l\pi) \\ & \times \sum_{i=0}^{1} \sum_{j=0}^{1} (-1)^{i+j} \alpha_{ij} H_{ij}(\omega_0, \omega_1) \\ & \cdot H_{ij}(\omega_0 + k\pi, \omega_1 + l\pi) \\ & + 4 \sum_{i=0}^{1} \sum_{j=0}^{1} (-1)^{i+j} H_{ij}(\omega_0, \omega_1) R_{ij}(2\omega_0, 2\omega_1).\end{aligned} \tag{23}$$

By analogy with the one-dimensional case we can again distinguish the four types of coding errors as defined in (18). The QMF error and the signal error are both filtered versions of the original 2D signal $X(\omega_0, \omega_1)$ and come from the first summation in (23), for $(k, l) = (0, 0)$. By definition, the QMF error consists of the difference between the original 2D signal $X(\omega_0, \omega_1)$ and the 2D reconstruction without coding errors, that is, when $\alpha_{ij} = 1$ and $R_{ij}(\omega_0, \omega_1) = 0$, for $i, j = 0, 1$. Since we use only separable 2D QMF's for splitting and reconstruction we employ this separability, yielding the 2D QMF error signal

$$\begin{aligned}E_Q(\omega_0, \omega_1) = {} & X(\omega_0, \omega_1) \\ & \times \{[H(\omega_0)^2 - H(\omega_0 + \pi)^2] \\ & \cdot [H(\omega_1)^2 - H(\omega_1 + \pi)^2] - 1\}.\end{aligned} \tag{24}$$

For the 2D signal error we take into account the α_{ij} val-

ues. Again using the separability of the 2D QMF $H(\omega_0, \omega_1)$ we get

$$\begin{aligned} E_S(\omega_0, \omega_1) &= [(\alpha_{00} - 1)H(\omega_0)^2H(\omega_1)^2 \\ &\quad - (\alpha_{01} - 1)H(\omega_0)^2H(\omega_1 + \pi)^2 \\ &\quad - (\alpha_{10} - 1)H(\omega_0 + \pi)^2H(\omega_1)^2 \\ &\quad + (\alpha_{11} - 1)H(\omega_0 + \pi)^2H(\omega_1 + \pi)^2]X(\omega_0, \omega_1). \end{aligned} \tag{25}$$

Note that the transfer function by which the signal $X(\omega_0, \omega_1)$ in (25) is multiplied, is not separable due to the values of α_{ij}, which in general are different. The aliasing error signal can be easily derived from (23) by taking the first summation for $(k, l) \neq (0, 0)$. We then obtain

$$\begin{aligned} E_A(\omega_0, \omega_1) &= [H(\omega_1)H(\omega_1 + \pi)][(\alpha_{00} - \alpha_{01})H(\omega_0)^2 \\ &\quad + (\alpha_{11} - \alpha_{10})H(\omega_0 + \pi)^2] \\ &\quad \times X(\omega_0, \omega_1 + \pi) \\ &\quad + [H(\omega_0)H(\omega_0 + \pi)][(\alpha_{00} - \alpha_{10})H(\omega_1)^2 \\ &\quad + (\alpha_{11} - \alpha_{01})H(\omega_1 + \pi)^2] \\ &\quad \times X(\omega_0 + \pi, \omega_1) \\ &\quad + [(\alpha_{00} - \alpha_{01} - \alpha_{10} + \alpha_{11})H(\omega_0) \\ &\quad \cdot H(\omega_0 + \pi)H(\omega_1)H(\omega_1 + \pi)] \\ &\quad \times X(\omega_0 + \pi, \omega_1 + \pi). \end{aligned} \tag{26}$$

Clearly, we can see that the aliasing error has three terms. This was to be expected, since each subband will have aliasing errors coming from the other three subbands, which are not completely compensated due to the coding errors. In this 2D case, the aliasing errors consist of the sum of two parts that have a 1D aliasing error in one direction and a 1D signal error in the other direction (the first two parts of (26)) and one part that has 1D aliasing errors in both directions (the last part of (26)). Finally, the random error consists entirely of the second summation in (23):

$$\begin{aligned} E_R(\omega_0, \omega_1) &= 4H_0(\omega_0)H_0(\omega_1)R_{00}(2\omega_0, 2\omega_1) \\ &\quad - 4H_0(\omega_0)H_1(\omega_1)R_{01}(2\omega_0, 2\omega_1) + \\ &\quad - 4H_1(\omega_0)H_0(\omega_1)R_{10}(2\omega_0, 2\omega_1) \\ &\quad + 4H_1(\omega_0)H_1(\omega_1)R_{11}(2\omega_0, 2\omega_1). \end{aligned} \tag{27}$$

According to (27) each subband coder/decoder produces its own uncorrelated quantizer noise, which is put into its corresponding frequency band due to the reconstruction filtering (ignoring the relatively small overlap between the frequency bands).

V. Experimental Results

The experimental analysis of quantization errors was performed for the subband coding schemes as previously described. The splitting scheme of Fig. 2 was used with the 16 tap filter denoted as 16B in [7]. To employ the same coding methods as in [5] and [13], we would have liked to use DPCM to encode the low frequencies subband. However, no useful input/output model is available for DPCM that is comparable to the gain-pulse-additive-noise model for Lloyd–Max quantization, (that is, with an uncorrelated additive noise term). Insertion of the model into a DPCM scheme would give us a noise signal which due to the feedback is not uncorrelated with the input signal. Therefore, we will use a Lloyd–Max quantizer for the subband containing the lowest frequencies as well, although the DPCM encoder would yield better coding results. For example, the drop in performance when the monochrome 512 × 512 image "Clown" is coded at 0.6 b/pixel is approximately 0.6 dB. The probability density function (pdf) on which the Lloyd–Max quantizer is based is Gaussian, which yielded a good match to the histogram of the subband, especially when compared to the occasionally used Laplacian or uniform pdf's. For the other subbands we employ the already designed and used quantizers that are based on the generalized Gaussian pdf with shape parameter $c = 0.5$.

To experimentally obtain the different error signals, first the image is split into subbands and the bit allocation algorithm [11] is applied. At that point the Lloyd–Max quantizers to be used are known and the value of α is computed using (8) for each subband. Applying the subband filters and the values of α the three error signals $E_Q(\omega)$, $E_S(\omega)$, and $E_A(\omega)$ can next be computed using (24), (25), and (26). The additive noise term per subband is calculated according to (5), by multiplying the original subband signal $\boldsymbol{x}$ by α and subtracting this from the actually encoded subband signal $\boldsymbol{y}$. Finally, the random error signal $E_R(\omega)$ is obtained using (27). Although (24) through (27) are for only four subbands they can easily be extended to the case where the image is split into more subbands.

We have performed experiments on several different images, which all lead to the same conclusions. As an example, we have taken the 512 × 512 image "Clown," of which the original is shown in Fig. 3. Fig. 4 shows the four different errors in the spatial domain when this image is encoded at 0.60 b/pixel. Because the variances of the resulting error images are very small when compared to the variance of the original image, each error image is stretched to maximum visibility. The signal error in Fig. 4(b) only occurs in high spatial frequency areas, such as edges. This was to be expected, since the lower frequency subbands are quantized more accurately than the higher frequency subbands, thus affecting the sharpness of edges.

The random error image in Fig. 4(d) still shows some features of the original image. This could imply that the quantization model of (5) does not produce a fully uncor-

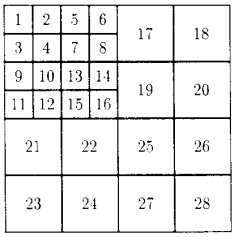

Fig. 2. Image frequency band division for subband coding of 512 × 512 images (zero frequency is at the upper left).

Fig. 3. Original 512 × 512 image "Clown."

related noise term, which can only be caused by a quantizer mismatch. To investigate the goodness of the quantizer fit, Table I shows the cross-correlation values between the original subband signals and the corresponding random signals for those subbands that are encoded. As can be seen, the correlation values are close to zero, pointing towards a good fit of the data to the Lloyd–Max quantizers. However, it can also be argued that even in the case of a perfect fit of the quantizers to the data, the random error will have a visual correspondence with the original image. While flat areas will be quantized using many similar quantization values, yielding a low local (random) error variance, on the other hand, edges and other high spatial frequency areas will result in a higher local error variance, thus yielding a visual resemblance to the original image. This effect can nevertheless also be attributed to quantizer mismatch, namely, to a spatially local quantizer mismatch. Observation of the random error image does indeed show a higher local variance in areas where the spatial frequency is relatively high. Another explanation for the visual correspondence to the original image would be the existence of nonlinear dependencies, being all but the linear (second moment) dependency, or correlation. In fact, in practice we never expect the random error image to look totally incoherent with the original image. Because we have a local quantizer mismatch, we expect the random error, and also the signal and the aliasing error to decrease when locally adaptive quantizers are used, thus enhancing the performance of a subband coder.

(a)

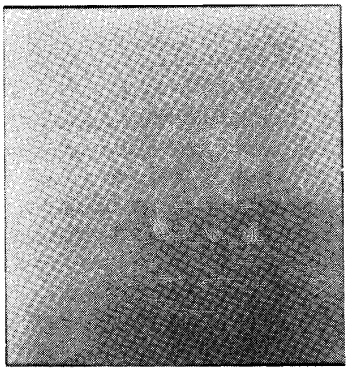

(b)

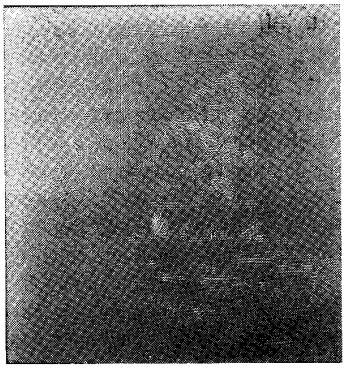

(c)

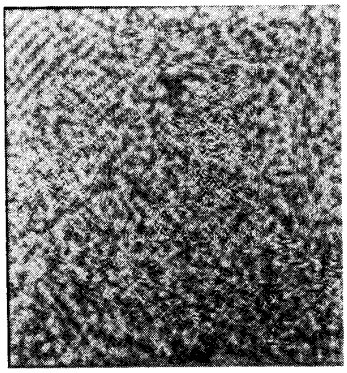

(d)

Fig. 4. Quantization errors (individually stretched): (a) QMF error, (b) signal error, (c) aliasing error, and (d) random error.

TABLE I
CROSS CORRELATIONS $E[xr]$ BETWEEN THE SUBBAND SIGNALS x AND THE SUBBAND ADDITIVE NOISE TERMS r

Subband	σ_x^2	α	σ_r^2	$E[xr]$
1	3927.49	0.9993	2.72	0.0396
2	77.18	0.9951	0.36	0.0628
3	67.20	0.9904	0.60	0.0803
4	19.19	0.9701	0.49	0.0324
5	7.04	0.8907	0.59	0.1171
6	50.76	0.9904	0.47	0.0070
7	2.94	0.8171	0.42	−0.1739
8	7.30	0.8907	0.61	0.0619
9	3.29	0.8171	0.49	0.1713
10	1.73	0.8171	0.26	0.0912
11	13.86	0.9701	0.36	0.1119
12	6.16	0.8907	0.55	0.0501
15	1.59	0.6371	0.33	−0.1805
16	3.57	0.8171	0.51	0.0864
18	6.45	0.6371	1.44	−0.303

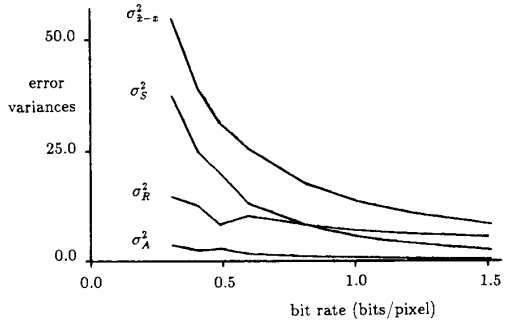

Fig. 5. Error variances as a function of the bit rate.

TABLE II
CROSS-CORRELATION MATRIX OF THE FOUR ERROR IMAGES

	E_Q	E_S	E_A	E_R
E_Q	1.0000	0.0136	0.0004	−0.0182
E_S	0.0136	1.0000	0.0213	−0.0002
E_A	0.0004	0.0213	1.0000	0.0022
E_R	−0.0182	−0.0002	0.0022	1.0000

The aliasing error in Fig. 4(c) and the QMF error in Fig. 4(a) both appear to have a very annoying character, when visible. However, if we look at Fig. 5, where the variances of the four error images are shown for a number of different bit rates, we can see that the signal error has a variance which is much larger than the aliasing error. In Fig. 5 the QMF error is even left out, because when compared to the other errors the variance is very small ($\sigma_Q^2 \approx 0.13$) and, moreover, bit rate independent. The signal error variance follows the curve of the total reconstruction error variance and is the largest in the low bit rate region (less than 0.8 b/pixel). For bit rates larger than 0.8 b/pixel the signal error becomes smaller than the random error. In that region, however, both the variances are so small that the errors in the reconstruction are hardly visible any more. Also from Fig. 5 it can be observed, that the sum of the separate error variances is close to the reconstruction error variance, suggesting uncorrelated error images. In fact, we expect the cross correlation between the random error image and the other three error images to be very low, because the Lloyd–Max quantizers produced output signals with (nearly) uncorrelated signal- and random parts, see Table I. In Table II the cross-correlation matrix is shown for the four error images, from which it can be deduced that the error images are, indeed, very much uncorrelated.

To investigate the subjective judgement of each of the coding errors, we have subtracted each error image from the actual reconstruction. In this case we have used the well-known 256 × 256 "Lady-with-hat" image, because the effects are more pronounced than with the Clown image and can therefore be observed more clearly. The same splitting scheme is used as in [13], [14], that is, the image is split into 16 equally sized subbands. Again, the QMF "16B" from [7] is used. The reconstruction at 0.60 b/pixel is shown in Fig. 6(a). Comparing this image with Fig. 6(b), the reconstruction minus the signal error, we see that the signal error mainly determines the sharpness. Examination of the reconstruction minus the random error in Fig. 6(d) shows a smoothed, somewhat unsharp version of the original image, with no visual artefacts in the flat areas or around the edges. Because the random error is particularly visible in the flat areas and the signal error is mainly around the edges and in the "busy" areas, both errors appear to have an equal subjective severity. However, the corresponding error variances in this case (0.60 b/pixel) have a similar behavior as in Fig. 5, where the signal error variance is larger than the random error variance. The reconstruction minus the aliasing error in Fig. 6(c) does not show any, or hardly any, visual difference from the reconstruction. The "muddy" appearance around the edges is still there and is therefore not an aliasing effect as one might expect but is due to the random error image. Once more it must be noted here, that the same effects can be observed in the Clown image, but the Lady-with-hat image merely serves as a better visual example.

Finally, to investigate the coder sensitivity to the type of filter used, in Table III the variances of the four error signals are shown for the different filters as designed in [7]. Also shown is the total mean-squared error, which is defined as the variance of the difference between the original image x and the reconstruction $\hat{x}$. For each filter the image Clown is encoded at 0.60 b/pixel. First, it can be observed that the signal error and the random error are nearly filter independent. The filter choice merely has its influence on the QMF design error and on the aliasing error. The total reconstruction error, which is close to the sum of the separate errors, is therefore also dependent on the type of filter used. For the filter 08A, which has 8 taps, both the QMF design error and the aliasing error are relatively large, and the reconstruction is clearly inferior to results with other (longer) filters. By visual inspection of difference images such as in Fig. 6(c), it is also apparent that the aliasing and QMF errors can not be neglected

Fig. 6. Visual impact of quantization errors for the 256 × 256 "Lady-with-hat" image: (a) reconstructed image $\hat{x}$, (b) $\hat{x} - e_S$, (c) $\hat{x} - e_A$, and (d) $\hat{x} - e_R$.

TABLE III
ERROR VARIANCES FOR DIFFERENT FILTERS

QMF	$\sigma^2_{\hat{x}-x}$	σ^2_Q	σ^2_S	σ^2_A	σ^2_R
08A	34.15	5.50	13.95	4.73	10.21
12A	26.59	0.39	13.75	2.44	9.84
12B	27.35	1.41	13.71	2.25	9.75
16A	25.43	0.05	13.72	1.91	9.72
16B	25.30	0.13	12.88	1.51	10.19
16C	26.69	1.75	12.72	1.76	10.03
24B	24.67	0.01	12.90	1.15	10.14
24C	23.34	0.01	12.54	1.04	9.34
24D	23.73	0.22	12.60	1.14	9.40
32C	23.19	0.00	12.61	0.86	9.37
32D	23.17	0.00	12.67	0.76	9.45
32E	24.48	0.88	12.72	1.11	9.54

for this filter. It is therefore recommended to use a filter with at least 12 taps. Here, we have used the best 16 tap filter 16B, because the performance is still substantially higher (and visible) than with the 12 tap filters, while using a 24 or 32 tap filter would increase coder complexity (number of multiplications) considerably, while the extra gain in performance is not visible in reconstructions.

VI. CONCLUSIONS

In the case of encoding each subband using a Lloyd–Max quantizer it is possible to use an input/output model for the quantizer, where the output consists of a signal part with a less than unity gain and a random part that is uncorrelated with the input signal. The measurement of the actual cross correlations between the random and the signal part of the model and also checking the noise variances per subband shows that the underlying probability density functions for which the quantizers were designed are based on a very good fit to the data.

Further, the introduction of the gain-plus-additive-noise quantizer model into QMF schemes yields the distinction between four different types of errors: QMF design error, signal error, aliasing error and random error. The QMF error, which is independent of the bit rate and thus of the coding errors, is insignificant and can be disregarded. Aliasing errors do occur in the case of quantization but can be neglected for filter lengths of 12 taps or more. The signal error determines the sharpness of the reconstructed image. The random error appears in flat regions but also around edges, though it is more pronounced and is therefore not entirely independent of the original image. Although for bit rates less than 0.8 b/pixel this error is less severe than the signal error with respect to the error variance, subjective evaluations have shown a more or less equal judgement of the two errors, though different in character. Finally, from the degree of visibility of the errors in different areas of the picture we can conclude that the performance of a subband coder is expected to im-

prove by reducing both the signal and the random error effects by means of applying spatially adaptive quantizers.

REFERENCES

[1] R. Ansari, S. H. Lee, and L. Wu, "Subband image coding using IIR filters," in *Proc. 1988 Conf. Inform. Sci. Syst.* (Princeton, NJ), Mar. 1988, pp. 16-21.

[2] T.-C. Chen and P. E. Fleischer, "Subband coding for ATV signals based on spatial domain considerations," *Proc. SPIE Int. Soc. Opt. Eng.*, vol. 1199, pp. 787-798, 1989.

[3] R. E. Crochiere, S. A. Webber, and J. L. Flanagan, "Digital coding of speech in subbands," *Bell Syst. Tech. J.*, vol. 55, no. 8, pp. 1069-1085, Oct. 1976.

[4] A. Croisier, D. Esteban, and C. Galand, "Perfect channel splitting by use of interpolation/decimation/tree decomposition techniques,"in *Proc. Int. Conf. Informat. Sci. Syst.* (Patras, Greece), pp. 443-446, Aug. 1976.

[5] H. Gharavi and A. Tabatabai, "Subband coding of digital images using two-dimensional quadrature mirror filtering," *Proc. SPIE Int. Soc. Opt. Eng.*, vol. 707, pp. 51-61, Sept. 1986.

[6] N. S. Jayant and P. Noll, *Digital Coding of Waveforms.* Englewood Cliffs, NJ: Prentice-Hall, 1984.

[7] J. D. Johnston, "A filter family designed for use in quadrature mirror filter banks," in *Proc. Int. Conf. Acoust., Speech, Signal Processing (ICASSP)* (Denver, CO), Apr. 1980, pp. 291-294.

[8] M. J. T. Smith and T. P. Barnwell, III, "Exact reconstruction techniques for tree-structured subband coders," *IEEE Trans. Acoust., Speech, Signal Processing*, vol. ASSP-34, no. 3, pp. 434-441, June 1986.

[9] P. P. Vaidyanathan, "Quadrature mirror filter banks, *M*-band extensions and perfect reconstruction techniques," *IEEE ASSP Mag.*, pp. 4-20, July 1987.

[10] M. Vetterli, "Multidimensional subband coding: Some theory and algorithms," *Signal Processing*, vol. 6, pp. 97-112, Apr. 1984.

[11] P. H. Westerink, J. Biemond, and D. E. Boekee, "An optimal bit allocation algorithm for subband coding," in *Proc. Int. Conf. Acoust., Speech, Signal Processing (ICASSP)* (New York, NY), Apr. 1988, pp. 757-760.

[12] P. H. Westerink, J. Biemond, and D. E. Boekee, "Quantization error analysis of image subband filter banks," in *Proc. Int. Symp. Circuits Syst. (ISCAS)* (Helsinki, Finland), June 1988, pp. 819-822.

[13] P. H. Westerink, J. Biemond, and D. E. Boekee, "Evaluation of image subband coding schemes," in *Proc. Europ. Signal Proc. Conf. (EUSIPCO)* (Grenoble, France), pp. 1149-1152, Sept. 1988.

[14] J. W. Woods and S. D. O'Neil, "Subband coding of images," *IEEE Trans. Acoust., Speech, Signal Processing*, vol. ASSP-34, no. 5, pp. 1278-1288, Oct. 1986.

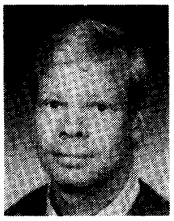

Peter H. Westerink (S'88-M'89) was born on October 5, 1961. He received the M.Sc. and Ph.D. degrees from the Delft University of Technology, the Netherlands, in 1985 and 1989, respectively.

Currently he is at AT&T Bell Laboratories, Murray Hill, NJ, working on algorithm development and software/hardware simulations of compression schemes for HDTV. His research interests include image coding, information theory, and (multidimensional) digital signal processing.

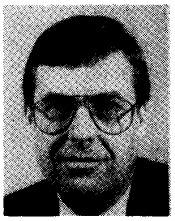

Jan Biemond (M'80-SM'87) was born in De Kaag, the Netherlands, on March 27, 1947. He received the M.S. and Ph.D. degrees in electrical engineering from the Delft University of Technology, Delft, the Netherlands, in 1973 and 1982, respectively.

He is currently a Professor in the Laboratory for Information Theory of the Department of Electrical Engineering at the Delft University of Technology. His research interests include multidimensional signal processing, image enhancement and restoration, data compression of images, and motion estimation with applications in image coding (HDTV) and computer vision. He has authored and coauthored numerous papers in these fields. In 1983 he was a Visiting Researcher at the Rensselaer Polytechnic Institute, Troy, NY, and at the Georgia Institute of Technology, Atlanta, GA.

Dr. Biemond is a member of the IEEE-ASSP Technical Committee on Multidimensional Signal Processing and a member of the IEEE-CAS Technical Committee on Visual Signal Processing and Communications. He has served as the General Chairman of the Fifth ASSP/EURASIP Workshop on Multidimensional Signal Processing, held at Noordwijkerhout, the Netherlands, in September 1987. He is Coeditor of the *International Journal on Multidimensional Systems and Signal Processing* and he serves on the Editorial Board of *Image Communication* and as AdCom member of the European Association for Signal Processing (EURASIP).

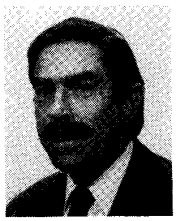

Dick E. Boekee (A'89) was born in the Hague, the Netherlands, in 1943. He received the M.Sc. and Ph.D. degrees in electrical engineering in 1970 and 1977, respectively, from the Delft University of Technology, Delft, the Netherlands.

In 1981 he became a Professor of Information Theory at the Delft University of Technology. During 1979-1980 he was a Visiting Professor at the Department of Mathematics, Katholieke Universiteit Leuven, Heverlee, Belgium. His research interests include information theory, image coding, cryptology, and signal processing.